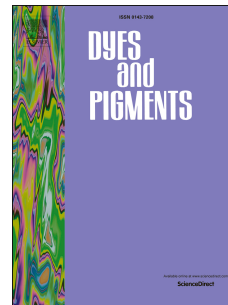


Accepted Manuscript

Gold nanoparticles modified by new conjugated S=C=N terminal and its biological imaging application

Anran Wang, Wan Sun, Cong Wang, Min Xu, Xin Lu, Xiaohe Tian, Shengli Li, Jieying Wu, Yupeng Tian



PII: S0143-7208(16)31249-9

DOI: [10.1016/j.dyepig.2017.02.004](https://doi.org/10.1016/j.dyepig.2017.02.004)

Reference: DYPI 5778

To appear in: *Dyes and Pigments*

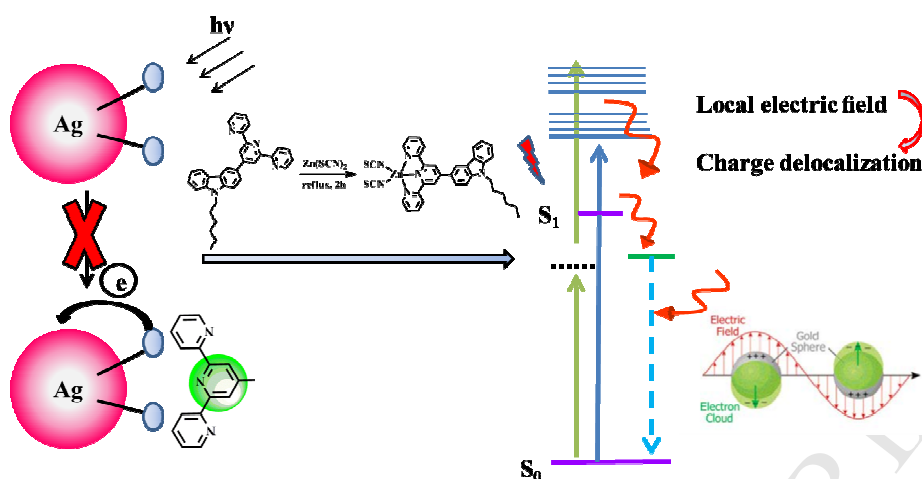
Received Date: 24 November 2016

Revised Date: 30 December 2016

Accepted Date: 2 February 2017

Please cite this article as: Wang A, Sun W, Wang C, Xu M, Lu X, Tian X, Li S, Wu J, Tian Y, Gold nanoparticles modified by new conjugated S=C=N terminal and its biological imaging application, *Dyes and Pigments* (2017), doi: 10.1016/j.dyepig.2017.02.004.

This is a PDF file of an unedited manuscript that has been accepted for publication. As a service to our customers we are providing this early version of the manuscript. The manuscript will undergo copyediting, typesetting, and review of the resulting proof before it is published in its final form. Please note that during the production process errors may be discovered which could affect the content, and all legal disclaimers that apply to the journal pertain.



Change PET to ICT through conjugated S=C=N modified by Gold nanoparticles

Gold nanostructures had recently become the most interesting areas of scientific endeavor. Herein, a novel nanostructure material was designed by S1 (2, 2': 6', 2''-terpyridyl derivative Zn(SCN)₂ complex) modified gold nanoparticles with obvious improving two photon absorption (TPA) cross section (σ), the fluorescence intensity, lifetime, fluorescence quantum yield due to the enhancement of intramolecular charge transfer (ICT) process. Compared with R1 (3-([2, 2': 6', 2''-terpyridin]-4'-yl) -9-hexyl-9H-carbazole), a conjugated ligand of carbazolyl styryl terpyridine derivatives, capping with Ag nanoparticles, photon induced electron transfer (PET) process led to the fluorescence quenching. The ¹H NMR study on the coordination reaction mechanism provided a new insight into the great mystery of nanoscience. Other related characterizations, such as IR and Far IR, could also prove the interaction of Au NPs and S1. The composite material with good nonlinear optical properties had potential applications in vitro cellular imaging.

Gold nanoparticles modified by new conjugated S=C=N terminal and its biological imaging application

Anran Wang^{‡a}, Wan Sun^{‡a}, Cong Wang^a, Min Xu^a, Xin Lu^a, Xiaohe Tian^b, Shengli Li^{*a},
Jieying Wu^a, Yupeng Tian^{*a}

^a Department of Chemistry, Anhui Province Key Laboratory of Functional Inorganic Materials, Anhui University, Hefei 230039, China;

^bSchool of Life Science, Center for Stem Cell Research and Translational Medicine. Anhui University, Hefei 230039, China

†Electronic Supplementary Information (ESI) available: See DOI: 10.1039/x0xx00000x

‡ These authors contributed equally.

Abstract

Gold nanostructures had recently become the most interesting areas of scientific endeavor. Herein, a novel nanostructure material was designed by S1 (2, 2': 6', 2''-terpyridyl derivative Zn(SCN)₂ complex) modified gold nanoparticles with obvious improving two photon absorption (TPA) cross section (σ), the fluorescence intensity, lifetime, fluorescence quantum yield due to the enhancement of intramolecular charge transfer (ICT) process. Compared with R1 (3-([2, 2': 6', 2''-terpyridin]-4'-yl)-9-hexyl-9H-carbazole), a conjugated ligand of carbazolyl styryl terpyridine derivatives, capping with Ag nanoparticles, photon induced electron transfer (PET) process led to the fluorescence quenching. The ¹H NMR study on the coordination reaction mechanism provided a new insight into the great mystery of nanoscience. Other related characterizations, such as IR and Far IR, could also prove the interaction of Au NPs and S1. The composite material with good nonlinear optical properties had potential applications in vitro cellular imaging.

Keywords: Gold nanoparticles; Two sulfur-terminal Zn(SCN)₂ complexes; Two-photon excited fluorescence; Biological imaging

1. Introduction

Design of chromophore-functionalized gold nanoparticles (NPs) with novel optical and physical properties had emerged as one of the most interesting areas of scientific endeavor over the past decades [1-5]. Carefully selecting the organics and metal species, tuning and optimizing their optical and plasmonic properties by a variation of their size, shape, surrounding environment and suited stabilizing agent could contribute to obtain Au NPs with high stability and overcome the limitations of fluorescence resonance energy transfer (FRET) and nonradiative electron transfer from photo-excited dye molecules to Au NPs relative to traditional quenchers [6-10]. Earlier, Li et al [11], Ray et al [12], Dana et al [13] and Ming et al [14] had reported the reason of emission enhancement of fluorophore in the presence of metal NPs due to the local electric field increasing when the metal surface plasmon band located between the absorption and emission band of the fluorophore [15]. This theory guided to improve for our earlier investigations that the fluorescence quenching had been demonstrated by energy and electron transfer between Ag NPs and terpyridine derivatives [16]. Two sulfur-terminal $Zn(SCN)_2$ complexes containing terpyridine group were chosen to be capped with gold nanoparticles according to the hard and soft acid-base theory.

Metal NPs had gained high interests in the field of nanomedicine such as biosensing, bioimaging and recently therapy [17-19]. Metal NPs were generally synthesized by a simple method using small organic molecules, polymeric or biological templates to stabilize them in solution [20]. Metal NPs exhibited molecular-like properties [21-22], long-lifetime fluorescence in the red-near-infrared region and large two-photon excitation. These properties made them highly suitable for *in vitro* and *in vivo* imaging [23-27]. What's more, the Au NPs capped with nonlinear optical materials exhibited more superior properties at the nonlinear optical fields and the cellular level with high permeability and low toxicity due to near-infrared radiation when compared with the pure metal NPs capped with polymeric or common

molecular [28-31]. Although the mechanism of the fluorescent enhancing was not fully understood, recent findings tended to confirm a coefficient contribution of quantum confinement in the metal core and ligand-to-metal charge transfer in the core-shell structure [32-34].

In the present investigation, to see the plasmon-exciton coupling effect and charge delocalization form of the photo-excited dye molecules on Au NP surface, two sulfur-terminal metal complexes containing terpyridine were chosen which had the relatively strong gold-thiolate (Au-S) bond and good NLO properties. Finally, a novel Au-complex composite material had been obtained with longer fluorescent lifetime, larger two-photon absorption (TPA) coefficient (β), TPA cross section (σ), nonlinear refractive index (γ) and third order nonlinear optical susceptibility ($\chi^{(3)}$) than the original complex. The further application was explored in cell imaging. The NLO material could be effectively penetrated into cellular cytoplasm with phenomenon in two-photon fluorescence microscopy towards HepG2 cells *in vitro*.

2. Experimental section

2.1 Measurements and methods

All chemicals were purchased as reagent grade and used without further purification. The solvents were dried and distilled according to standard procedures. IR spectra (4000-400 cm^{-1}), in KBr pressed pellets, were recorded on a Nicolet FT-IR 170 SX spectrophotometer. $^1\text{H-NMR}$ spectra were performed on a Bruker 500Hz Ultrashield spectrometer and reported as parts per million (ppm) from TMS (δ). Coupling constants J are given in Hertz. UV-vis absorption spectra were measured on a UV-265 spectrophotometer. The fluorescence spectra in solution were performed with an F-4500 fluorescence spectrophotometer. The concentration of sample solution was 1.0×10^{-5} M. The morphologies were obtained on transmission electron microscope (TEM, JEM-2100). Fluorescence lifetime measurements were carried out using an HORIBA FluoroMax-4P fluorescence spectrometer equipped with a

time-correlated single-photon counting (TCSPC) card. NLO properties were measured by a femtosecond laser pulse and Ti: 95 sapphire system (680~1080 nm, 80 MHz, 140 fs, Chameleon II) as the light source, and all measurements were carried out at room temperature. Zeta Potentials were measured by using a zeta sizer ((Nano ZS90, Malvern Instruments, UK)) at a temperature of 25°C.

2.2 Synthetic procedures

2.2.1. Synthesis of R1

The preparation of 3-([2, 2': 6', 2''-terpyridin]-4'-yl)-9-hexyl-9H-carbazole (R1) was carried out according to the reported article of previous work [35], as shown in **Scheme 1** and the relative characterizations were examined to meet the purity requirement.

2.2.2. Synthesis of R1-Ag NPs

Sodium borohydride were known to be strong reducing agents and suitable for metal ion reduction. The R1-Ag NPs were obtained by the reduction of AgNO₃ with NaBH₄ in DMF solution using R1 as the stabilizing agent (**Scheme 1**). In more detail, R1 powder (0.0964 g, 0.2 mmol) was first dissolved in DMF (100 mL). Then, AgNO₃ (0.1265 g, 0.5mmol) dissolved in DMF (50 mL) was added into the solution with magnetic stirring at room temperature for 30 min. In this step, Ag⁺ ions and R1 formed translucent R1-Ag⁺ sol, and the mixture color changed from colorless to brilliant yellow. Next, 12 mL freshly prepared DMF solution containing 0.01M NaBH₄ was added into the above sol and instantly a pale yellow solution generated. Sequentially, the mixtures were stirred for another 60 min. The color change indicated that the Ag⁺ ions were reduced. Finally, the products were collected by centrifugation of the precipitate, washed with distilled water-DMF mixture several times and then dried in vacuum oven.

2.2.3. Synthesis of 3-([2, 2':6', 2''-terpyridin]-4'-yl)-9-hexyl-9H-carbazole Zn (SCN)₂ complex (S1)

As shown in **Scheme 2**, R1 (0.193 g, 0.4 mmol) was dissolved in 5 mL CH₂Cl₂, in which 10 mL CH₃OH containing Zn(SCN)₂ (0.073 g, 0.4 mmol) was added with refluxing at 70°C for 2h. Cooled to the room temperature, bright yellow product was crystallized from the filtered solution. ¹H NMR (DMSO-d₆, 400 MHz) (ppm): 0.82(m, 3H), 1.30(d, 6H), 1.82(s, 2H), 4.49(m, 2H), 7.33(m, 1H), 7.55(m, 2H), 7.69(m, 1H), 7.86-7.96(m, 3H), 8.33-8.43(m, 4H), 8.84(s, 2H), 9.06(s, 1H), 9.13-9.18(m, 3H). MS (GCT-MS), C₃₅H₃₀ZnN₆S₂: 662.13, found: 603.18 [M⁺]. The crystal structure of S1 was shown in **Figure. S1**.

2.2.4 Synthesis of S1-Au NPs

In a typical reaction, as shown in **Scheme 2**, the following conditions were used to prepare the Au NPs. An amount of 326 μL (7.92×10⁻⁶ mol) of 24.3 mM tetrachloroauric(III) acid (HAuCl₄·3H₂O) stock solution and the desired molar concentration of S1 were dissolved in 25 mL DMF. The mixture was then stirred at room temperature for 1 h, which was based on the anticipated minimum time necessary to promote precursor formation (see below). An amount of 72 μL (6.3×10⁻⁵ mol) of 880 mM sodium borohydride (NaBH₄) stock solution in DMF was added over 30 min with vigorous stirring. To prepare different size of nanoparticles, the molar concentration of HAuCl₄ was fixed and the amount of S1 was varied. With the following addition of reducing agent, the color of the mixture immediately changed to brown or red depending on the nanoparticle size. The mixture was then left stirring for at least 3 h and it gradually progressed to final appearance. ¹H NMR (DMSO-d₆, 400 MHz) (ppm): 0.82(m, 3H), 1.30(d, 6H), 1.82(s, 2H), 4.49(m, 2H), 7.33(m, 1H), 7.55(m, 2H), 7.69(m, 1H), 7.86-7.96(m, 3H), 8.33-8.43(m, 4H), 8.90(s, 2H), 9.04-9.06 (d, 2H), 9.17-9.21(d, 2H).

Scheme 1 Synthetic route for R1, R1-Ag NPs.**Scheme 2** Synthetic route for S1, S1-Au NPs**3. Results and discussion***3.1 Characterizations of R1, S1, R1-Ag NPs and S1-Au NPs*

These common characterizations of TEM, XRD, DLS, ^1H NMR, IR and Far-IR of R1, S1, R1-Ag NPs and S1-Au NPs were shown in Supporting information.

3.2. Absorption and emission spectroscopy of R1-Ag NPs

The absorbance properties of R1 and R1-Ag NPs were first studied. As shown in **Figure. 1**, two major absorption bands in the range of 250~500 nm were observed. The ligand peaks 309 nm and 360 nm could be assigned to π - π^* transition and ICT, blue shifted to 294 nm and 338 nm for the modified NPs, respectively. Localized surface plasma resonance (LSPR) band of Ag nanoparticles located at about 400nm and red shifted with the time, indicating that the electrons of silver nanoparticles (Ag NPs) transferred to ligand and led to density increasement of R1.

The fluorescence emission peak of R1 displayed at 428 nm (**Figure. 1**). Meanwhile, the emission peak of R1-Ag NPs shifted to 525 nm and quenched, suggesting that there was a fast energy transfer and electron transfer from Ag NPs to ligand R1. It was different with our assumption, so the S1-Au NPs composite was designed and their optical properties were described below according to Anger's theory.

Fig. 1. UV-vis spectrograms and fluorescence spectra of R1, R1-Ag NPs*3.3 Absorption spectroscopy of S1-Au NPs*

Prior to demonstrate the excited state behavior, it was necessary to examine the ground state interaction between S1 and Au NPs. **Figure. S8**

showed the absorption spectra of S1-Au NPs, in which the localized surface plasmon resonance (LSPR) band located at about 530 nm and red shifted with the increase of the ratio. The band at 393 nm was assigned to ICT of S1-Au NPs, red shifted imperceptibly when compared with free S1 (390 nm), due to their strong coupling with surface plasmon of Au Nanoparticles [36].

The time-dependent UV-vis absorption spectrum for S1-Au NPs with the ratio 1:1 was shown in **Figure. 2**. The peak of ICT decreased and red shifted. The LSPR band enhanced with time increasing, showing the composite process of S1 and gold particles. S1 perfectly composited with gold nanoparticles [37].

Fig. 2. Time-dependent UV-vis absorption spectra for S1-Au NPs (S1: Au=1:1)

3.4. Emission spectroscopy of S1-Au NPs

To investigate the molecular interaction and plasmonic resonances of Au NPs, emission spectroscopy had been carried out for S1-Au NPs. **Figure. 3** showed the emission spectra of S1 with Au NPs in different concentration. Here, the concentration of S1 was $1 \times 10^{-5} \text{ mol} \cdot \text{L}^{-1}$, the molar concentration of HAuCl_4 was fixed and the amount of S1 was varied. The concentration of S1-Au NPs was determined by the ratio. It was interesting to see that, in the presence of 1:1, the emission peak at 541 nm was enhanced and blue shifted to 520nm, even part of spectral overlap between the molecular emission and absorption of the surface plasmon. Energy transfer might take place in the S1-Au NPs system, and the emission enhancement of fluorophore could proceed in the presence of metal NPs. It proved the reason was the enhanced local electric field, while the surface plasmon band of nano metal particles lied in between the absorption band and emission band of the fluorophore [11].

The different emission peaks of S1-Au NPs located at 532 nm, 519 nm, 504 nm and 503 nm, respectively, with the ratio increase of S1 to Au. S1-Au NPs composites were excited at 400 nm with blue region of the plasmon band.

So emission enhancement could not be attributed to optical enhancement [38]. To understand the reason of emission intensity increment of S1 on Au NPs, surface time-resolved emission had been studied and described in the next section.

Fig. 3. Fluorescence spectra of S1-Au NPs (S1: Au =1:0.1, 1:1, 1:50, 1:500, 1:5000) and S1

3.5. Time-resolved emission spectroscopy of S1-Au NPs

Figure. 4 showed the fluorescence decay of S1 and S1-Au NPs, and the solid samples were dissolved in DMF. The average emission lifetime of S1 was 2.51 ns, attributed to the lifetime of ICT state. The emission decay lifetime of S1-Au NPs was 5.08ns could also be traced derived from the ICT process. Meanwhile, the luminescence quantum yields (QY) were shown in **Table 1**. QY of S-Au NPs was enhanced from 9.77% to 23.32%. From luminescence quantum yields and time-resolved emission studies, it was confirmed that there was no energy transfer from photo-excited S1 to Au NPs. This indicated a drastic increment of emission due to the ICT effect of S1 on Au NPs surface.

Further, the ability of Au NPs to store and transfer electrons increased the attenuation number and extended the decay time. The coupled effect for surface plasmon could lead to enhancing the stability of the excited state and decreasing the total radiation attenuation rate [39].

Fig. 4. The fluorescence lifetime of S1 and S1–Au NPs

Table 1. Single-photon-related photo physical properties of R1, R1-Ag NPs, S1 and S1-Au NPs

3.6. Solvation effect of S1-Au NPs

Significantly, the S1-Au NPs could easily disperse in common organic solvents and exhibit a strong solvent-resolved fluorescence. **Figure. 5** showed the emission spectra of S1-Au NPs in seven solvents with different polarities. The emission maximum displayed an obvious red shift upon increasing the solvent polarity. There may be great changes in the molecular geometry of the excited states before fluorescence emission. The fluorescence deviation in solution could be attributed to the dipolar interaction between the solute and the local solvent.

Fig. 5. Normalized fluorescence spectra of S1 (left) and S1-Au NPs (right) in different solvents

3.7. Nonlinear optical properties of S1 and S1-Au NPs

In the linear absorption spectra (see **Figure. 2**), it was discovered that there was no linear absorption in the wavelength range 680-910 nm for the two-photo materials. Therefore, any emission induced by excitation at this wavelength range should be derived from multiphoton absorption process.

By the open and closed Z-scan test methods, the nonlinear refractive index (γ), nonlinear absorption coefficient (β), TPA cross section (σ) and third order nonlinear susceptibility ($\chi^{(3)}$) were shown in **Table S1.** and **Figure. 6a, b.** The calculation process was given in **S2.** It was shown that the TPA cross section (σ) enhanced from 13368.5 GM to 16298.01 GM without the influence of pure nano gold ($\sigma=2874.2$ GM, **Figure. S9, Table S1.**). The third order nonlinear susceptibility ($\text{Re}(\chi^{(3)})[\text{esu}]$) enhanced from 1.24×10^{-12} to 1.24×10^{-11} , for the increased chromophore density in the complex shell might lead to increasing the σ_{TPA} [40]. In view of the above advantages, it could be concluded that the coupling interactions and the corresponding exciton plasmon interactions between the Au and S1 had significant contribution to the enhancement of TPA [41], which stimulated the research to further explore its potential application in biological imaging. **Figure. 6c** reported the optical limiting (OL) measurements

for the S1-Au NPs, carried out with 790 nm laser pulses. When the input energy reached about 0.48 J/cm^2 , the transmitted energy started to deviate from the normal line and exhibits a typical limiting effect. The damaging threshold was 0.98 J/cm^2 , suggesting that this composite was a good candidate compared to C_{60} , which was considered as one of the best optical limiting materials [42].

Fig. 6. Open (a), closed (b) aperture Z-scan curves, optical limiting (c) of S1 and S1-Au NPs in DMF ($c = 1.0 \times 10^{-3} \text{ mol}\cdot\text{L}^{-1}$)

3.8. Application in bioimaging

Before exploring the biological applications, cytotoxicity of the nanoparticles were measured toward the live human hepatocellular liver carcinoma cells (HepG2) by MTT assay shown in **Figure. S10**. The result indicated that the concentration from 10 to 100 mg/L of S1 and S1-Au NPs exhibited low cytotoxicity.

As shown in **Figure. 7**, one- and two-photon fluorescent confocal microscopy of HepG2 cells labeling with S1 and S1-Au NPs were captured. A bright-field image of each cell was taken immediately prior to one- and two-photon microscopy (2 PM) imaging. One-photon images of HepG2 cells incubated with 20 mg/L S1 ($\lambda_{\text{ex}} = 540 \text{ nm}$) and S1-Au NPs ($\lambda_{\text{ex}} = 520 \text{ nm}$), respectively. After 30 min of incubation, washed by PBS buffer, all the emission wavelengths were from 500 to 560 nm. Two-photon images of S1 and S1-Au NPs ($\lambda_{\text{ex}} = 800 \text{ nm}$, $\lambda_{\text{em}} = 540\text{-}600 \text{ nm}$) were obtained by the same process. The results indicated that the free complex S1 did not enter the cell and S1-Au NPs evenly into the cells. The luminescence located in cell cytosol, supposing that the S1-Au NPs permeated the phospholipids bilayer of cellular membrane and bounded with cellular cytosol organelle. The colocalization imaging and 3D image of S1-Au NPs (**Figure. 7**) could detect more clearly the cellular targeted situation.

Fig. 7. One- and two-photon fluorescence microscopy image of HepG2 cells incubated with S1, S1-Au NPs (scale bar: 20 μ m); two-photon fluorescence colocalization imaging (bar: 5 μ m) and 3D image of S1-Au NPs incubated with Syto9 (commercial dyes) ($\lambda_{\text{ex}}=488$ nm, $\lambda_{\text{em}}=550$ nm).

4. Conclusion

We designed and characterized the two-photon chromophore-functionalized gold nanostructure, which one-photon fluorescence intensity enhancing approximately 26 times than the original dye. By studying the time-dependent absorption and time-resolved emission decay of the free complex and S1-Au NPs, the reason why fluorescence enhancement for S1-Au NPs is coupled effect of local electric field enhancement and surface plasmon of Au nanoparticles. The corresponding exciton plasmon interactions between the components S1 and Au NPs led to a larger TPA cross section in the near-IR region. The decorated gold nanoparticles could effectively penetrate into living cells and stained with cytosol, indicating that the composite might be a potential excellent material in bioimaging applications.

Acknowledgments

This work was supported by a grant for the National Natural Science Foundation of China (21271004, 51372003, 21271003, 51432001, 21101001), the Anhui Provincial Natural Science Foundation (1308085MB24) and Scientific Innovation Team Foundation of Educational Commission of Anhui Province of China (KJ2012A025, 2006KJ007TD).

References

[1] X. Li, F. Zhang, D. Zhao

Lab on unconversion nanoparticles: optical properties and applications engineering via designed nanostructure

Chem. Soc. Rev., 44 (2015), pp. 1346-1378

[2] T. Zou, C. T. Lum, C. N. Lok, J. J. Zhang, C. M. Che

Chemical biology of anticancer gold (III) and gold (I) complexes

- Chem. Soc. Rev., 44 (2015), pp. 8786-8801
- [3] M. Zhao, Y. Zhuo, Y. Q. Chai, R. Yuan
Au nanoparticles decorated C 60 nanoparticles-based label-free electrochemiluminescence aptasensor via a novel “on-off-on” switch system
Biomaterials, 52 (2015), pp. 476-483
- [4] J. Huang, L. Lin, D. Sun, H. Chen, D. Yang, Q. Li
Bio-inspired synthesis of metal nanomaterials and applications
Chem. Soc. Rev., 44 (2015), pp. 6330-6374
- [5] J. Owen
The coordination chemistry of nanocrystal surfaces
Science, 347 (2015), pp. 615-616
- [6] P. V. Kamat, S. Barazzouk, S. Hotchandani
Electrochemical Modulation of Fluorophore Emission on a Nanostructured Gold Film
Angew. Chem. Int. Ed, 41 (2002), pp. 2764-2767
- [7] W. Shi, Y. Sahoo, M. T. Swihart, P. N. Prasad
Gold Nanoshells on Polystyrene Cores for Control of Surface Plasmon Resonance
Langmuir, 21 (2005), pp. 1610-1617
- [8] S. Mayilo, M. A. Kloster, M. Wunderlich, A. Lutich, T. A. Klar, A. Nichtl, K. Kurzinger, F. D. Stefani, J. Feldmann
Long-Range Fluorescence Quenching by Gold Nanoparticles in a Sandwich Immunoassay for Cardiac Troponin T
Nano letters., 9 (2009), pp. 4558-4563
- [9] F. C. M. Leung, A. Y. Y. Tam, V. K. M. Au, M. J. Li, V. W. W. Yam
Forster Resonance Energy Transfer Studies of Luminescent Gold Nanoparticles Functionalized with Ruthenium (II) and Rhenium (I) Complexes: Modulation via Esterase Hydrolysis
ACS Appl. Mater. Inter., 6 (2014), pp. 6644-6653
- [10] P. C. Ray, A. Fortner, G. K. Darbha
Gold Nanoparticle Based FRET Assay for the Detection of DNA Cleavage

- J. Phys. Chem. B, 110 (2006), 20745-20748
- [11] X. Li, F. J. Kao, C. C. Chuang, S. He
Enhancing fluorescence of quantum dots by silica-coated gold nanorods under one-and two-photon excitation
Opt. Express, 18 (2010), pp. 11335-11346
- [12] Pay, Y. E. K. Lee, G. Kim, R. Kopelman
Two-Photon Fluorescence Imaging Super-Enhanced by Multishell Nanophotonic particles, with Application to Subcellular PH
Small, 8 (2012), pp. 2213-2221
- [13] J. Dana, T. Debnath, P. Maity, H. N. Ghosh
Restriction of Molecular Rotation and Intramolecular Charge Distribution in the Photoexcited State of Coumarin Dyes on Gold Nanoparticle Surface
The Journal of Physical Chemistry C, 119 (2015), pp. 2046-2052
- [14] T. Ming, H. Chen, R. Jiang, Q. Li, J. Wang
Plasmon-Controlled Fluorescence: Beyond the Intensity Enhancement
J. Phys. Chem. Lett., 3 (2012), pp. 191-202
- [15] J. Haes, S. L. Zou, J. Zhao, G. C. Schatz, R. P. Van Duyne
Localized surface plasmon resonance spectroscopy near molecular resonances
J. Am. Chem. Soc., 128 (2006), pp. 10905-10914
- [16] W. Sun, Y. Z. Zhu, A. R. Wang, L. Kong, S. L. Li, J. Y. Wu, Y. P. Tian
Formation and nonlinear optical properties of Ag nanocrystals capped with the conjugated ligand carbazolyl styryl terpyridine[†]
New J. Chem., 39 (2015), pp. 6830-6835
- [17] L. Zhang, E. Wang
Metal nanoclusters: New fluorescent probes for sensors and bioimaging
Nano Today, 9 (2014), pp. 132-157
- [18] L. Shang, F. Stockmar, N. Azadfar, G. U. Nienhaus
Intracellular Thermometry by Using Fluorescent Gold Nanoclusters[‡]
Angew. Chem. Int. Ed, 52 (2013), pp. 11154-11157
- [19] J. Liu, M. Yu, C. Zhou, S. Yang, X. Ning, J. Zheng

Passive Tumor Targeting of Renal-Clearable Luminescent Gold Nanoparticles: Long Tumor Retention and Fast Normal Tissue Clearance

J. Am. Chem. Soc., 135 (2013), pp. 4978-4981

[20] J. Zheng, C. Zhou, M. Yu, J. Liu

Different sized luminescent gold nanoparticles

Nanoscale, 4 (2012), pp. 4073-4083

[21] R. Jin

Quantum sized, thiolate-protected gold nanoclusters

Nanoscale, 2 (2010), pp. 343-362

[22] D. E. Jiang

The expanding universe of thiolated gold nanoclusters and beyond

Nanoscale, 5 (2013), pp. 7149-7160

[23] L. Shang, K. Nienhaus, X. Jiang, L. Yang, K. Landfester, V. Mailander, T. Simmet, G. Nienhaus

Nanoparticle interactions with live cells: Quantitative fluorescence microscopy of nanoparticle size effects

Nanotechnol., 5 (2014), pp. 2388-2397

[24] C. L. Liu, M. L. Ho, Y. C. Chen, C. C. Hsieh, Y. C. Lin, Y. H. Wang, M. J. Yang, H. S. Duan, B. S. Chen, J. F. Lee, J. K. Hsiao, P. T. Chou

Thiol-Functionalized Gold Nanodots: Two-Photon Absorption Property and Imaging In Vitro

J. Phys. Chem. C, 113 (2009), pp. 21082-21089

[25] X. Le Guevel, V. Trouillet, C. Spies, K. Li, T. Laaksonen, D. Auerbach, G. Jung, M. Schneider

High photostability and enhanced fluorescence of gold nanoclusters by silver doping

Nanoscale, 4 (2012), pp. 7624-7631

[26] F. Aldeek, M. A. H. Muhammed, G. Palui, N. Zhan, H. Mattoussi

Growth of Highly Fluorescent Polyethylene Glycol- and Zwitterion-Functionalized Gold Nanoclusters

ACS Nano, 7 (2013), pp. 2509-2521

- [27] E. Oh, F. K. Fatemi, M. Currie, J. B. Delehanty, T. Pons, A. Fragola, S. Leveque-Fort, R. Goswami, K. Susumu, A. L. Huston, I. L. Medintz
PEGylated Luminescent Gold Nanoclusters: Synthesis, Characterization, Bioconjugation, and Application to One- and Two-Photon Cellular Imaging
Part. Syst. Charact., 30 (2013), pp. 453-466
- [28] K. Cheng, S. R. Kothapalli, H. Liu, A. L. Koh, J. V. Jokerst, H. Jiang, M. Yang, J. Li, J. Levi, J. C. Wu, S. S. Gambhir, Z. Cheng
Construction and Validation of Nano Gold Tripods for Molecular Imaging of Living Subjects
J. Am. Chem. Soc., 136 (2014), pp. 3560-3571
- [29] M. Martinez-Calvo, K. N. Orange, R. B. P. Elmes, B. C. Poulsen, D. C. Williams, T. Gunnlaugsson
Ru(II)-polypyridyl surface functionalised gold nanoparticles as DNA targeting supramolecular structures and luminescent cellular imaging agents†
Nanoscale, 8 (2016), pp. 563–574
- [30] J. B. Qin, Z. Y. Peng, B. L. K. Ye, Y. X. Zhang, F. K. Yuan, X. R. Yang, L. J. Huang, J. Q. Hu, X. W. Lu
Gold nanorods as a theranostic platform for in vitro and in vivo imaging and photothermal therapy of inflammatory macrophages†
Nanoscale, 7 (2015), pp. 13991–14001
- [31] X. Yang, M. Yang, B. Pang, M. L. Vara, Y. N. Xia
Gold Nanomaterials at Work in Biomedicine
Chem. Rev., 115 (2015), pp. 10410-10488
- [32] J. Zheng, P. R. Nicovich, R. M. Dickson
Highly Fluorescent Noble Metal Quantum Dots
Rev. Phys. Chem, 58 (2007), pp. 409-431
- [33] Z. Wu, R. Jin
On the Ligand's Role in the Fluorescence of Gold Nanoclusters
Nano Lett, 10 (2010), pp. 2568-2573
- [34] X. Le Guevel, O. Tagit, C. E. Rodríguez, V. Trouillet, M. Pernia Leal, N. Hildebrandt,

Ligand effect on the size, valence state and red/near infrared photoluminescence of bidentate thiol gold nanoclusters

Nanoscale, 6 (2014), pp. 8091-8099

[35] L. F. Xiao, H. Wang, Q. Zhang, Y. Z. Zhu, J. Y. Wu, Y. P. Tian

Novel ruthenium (II) polypyridyl complexes containing carbazole with flexible substituents: Crystal structure, nonlinear optical properties and DNA-binding interaction

Dyes and Pigments, 113 (2015), pp. 165-173

[36] T. E. Karam, L. H. Haber

Molecular adsorption and resonance coupling at the colloidal gold nanoparticle interface

J. Phys. Chem. C, 118 (2014), pp. 642-649

[37] Y. Gao, J. Wu, Q. Zhao, L. Zheng, H. Zhou, S. Zhang, J. Yang, Y. Tian,

Solvent-resolved fluorescent Ag nanocrystals capped with a novel terpyridine-based dye

New J. Chem., 33 (2009), pp. 607-611

[38] T. Ming, H. Chen, R. Jiang, Q. Li, J. Wang

Plasmon-controlled fluorescence: beyond the intensity enhancement

J. Phys. Chem. Lett., 3 (2012), pp. 191-202

[39] (a) A. Kotiaho, R. Lahtinen, H. Lehtivuori, N. V. Tkachenko, H. Lemmetyinen

Photoinduced charge and energy transfer in phthalocyanine-functionalized gold nanoparticles

J. Phys. Chem. C, 112 (2008), pp. 10316-10322

(b) J. Lee, P. Hernandez, J. Lee, A. O. Alexander, N. A. Kotov

Exciton-plasmon interactions in molecular spring assemblies of nanowires and wavelength-based protein detection

Nat. Mater, 6 (2007), pp. 291-295

[40] F. Stellacci, C. A. Bauer, T. Meyer-Friedrichsen, W. Wenseleers, S. R. Marder, J. W.

Perry

Ultrabright supramolecular beacons based on the self-assembly of two-photon chromophores on metal nanoparticles

J. Am. Chem. Soc., 125 (2003), pp. 328-329

- [41] H. W. Dai, Y. Yu, X. Wang, Z. W. Ma, C. Chen, Z. K. Zhou, J. B. Han, Y. B. Han, S. D. Liu, L. Li

Study of Surface Plasmon Induced Hot Electron Relaxation Process and Third-Order Optical Nonlinearity in Gold Nanostructures

J. Phys. Chem. C, 119 (2005), pp. 27156-27161

- (b) K. Zhang, Z. L. Huang, H. W. Dai, Z. W. Ma, J. B. Han, H. M. Gong, Y. B. Han

[HTML] Surface plasmon enhanced third-order optical nonlinearity of silver nanocubes

Opt. Mater. Express, 5 (2015), pp. 2648-2654

- [42] V. Amendola, D. Dini, S. Polizzi, J. Shen, K. M. Kadish, M. J. F. Calvete, M. Hanack, M. Meneghetti

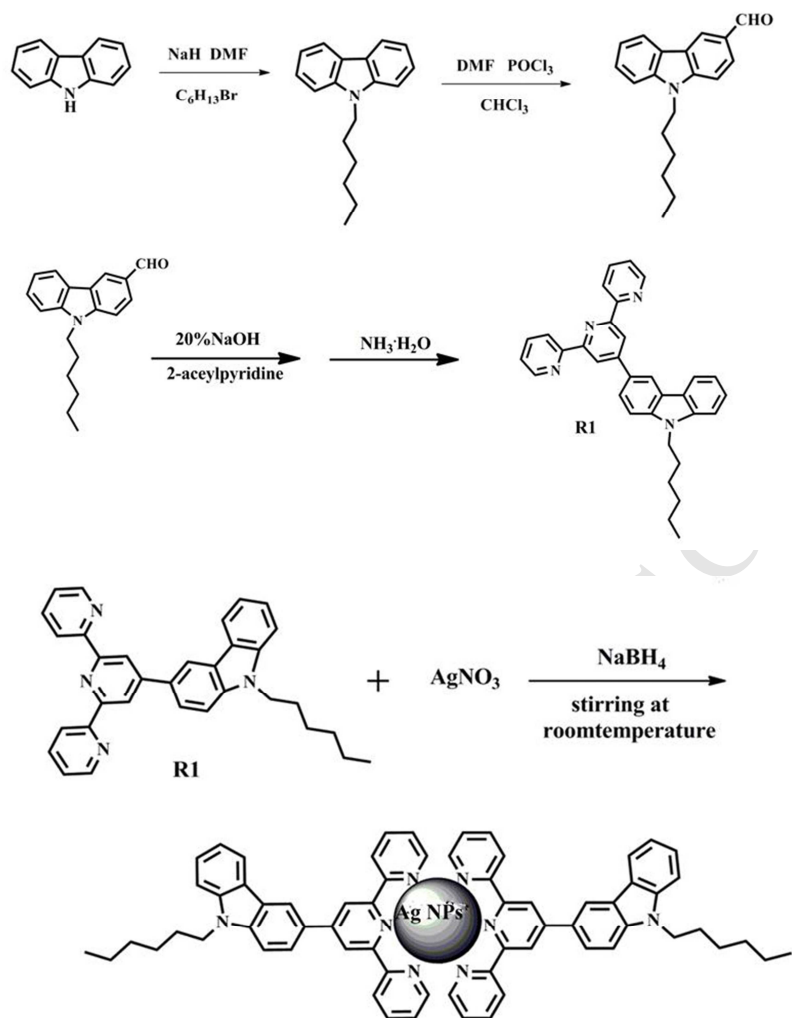
Self-healing of gold nanoparticles in the presence of zinc phthalocyanines and their very efficient nonlinear absorption performances

J. Phys. Chem. C, 113 (2009), pp. 8688-8695

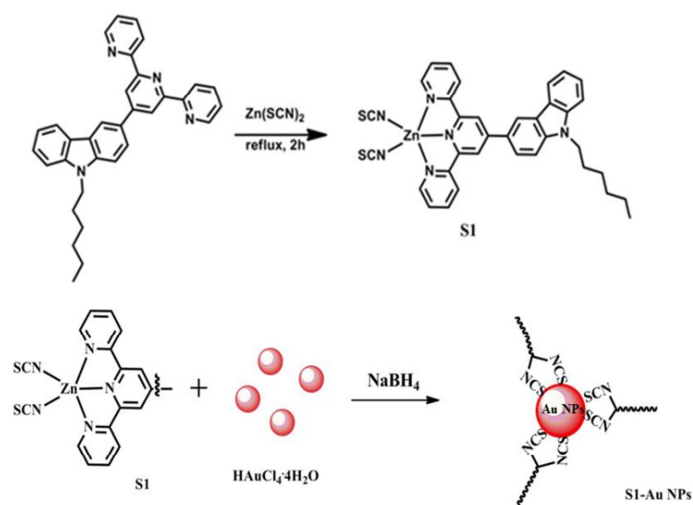
Table 1 Single-photon-related photo physical properties of R1, R1-Ag NPs, S1 and S1-Au NPs

compound	solvent	$\lambda_{\max}^{[a]}$	τ	$\lambda_{\max}^{[b]}$	$\Phi^{[c]}$
R1	DMF	309, 357	4.98	428	3.69
R1-Ag NPs	DMF	294, 338, 420	4.83	520	--
S1	DMF	318, 390	2.51	541	9.77
S1-Au NPs	DMF	329, 393, 530	5.08	520	23.32

[a] Peak position of the absorption band; [b] Peak position of single-photon fluorescence, excited at the absorption maximum; [c] Quantum yields determined by using fluorescein as standard.



Scheme 1 Synthetic routes for R1 and R1-Ag NPs.



Scheme 2 Synthetic routes for S1 and S1-Au NPs.

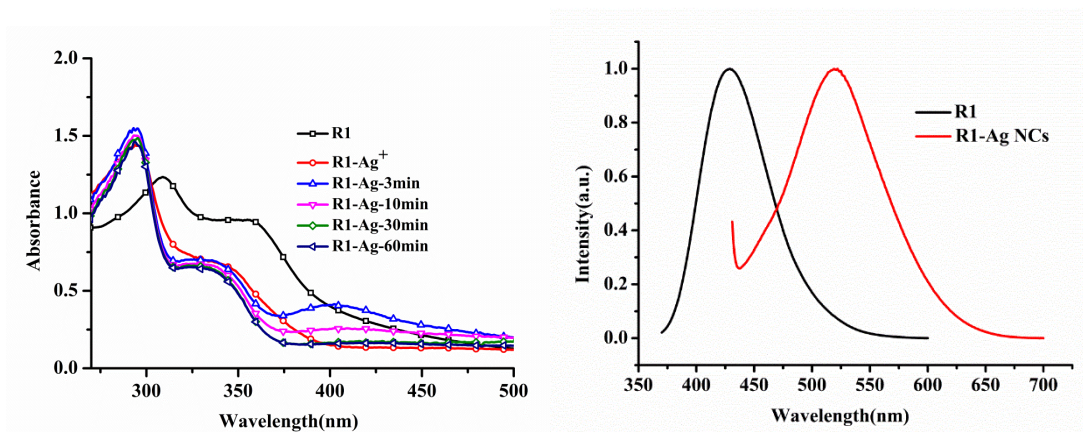


Figure 1 UV-vis absorption spectra and fluorescence spectra of R1 and R1-Ag NPs.

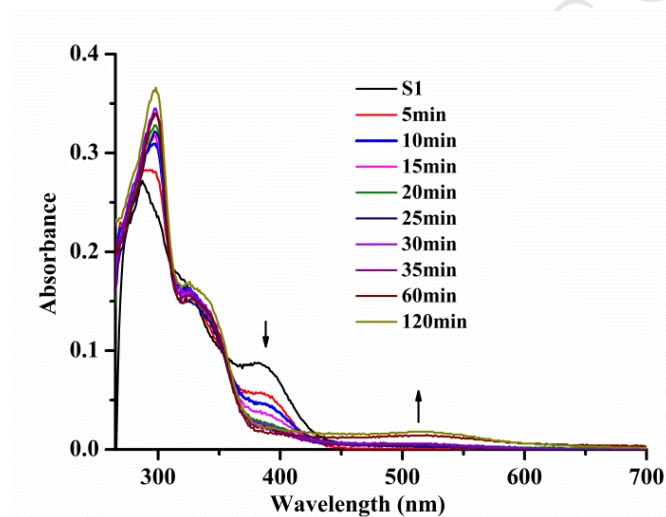


Figure 2 Time-dependent UV-vis absorption spectra for S1-Au NPs (S1: Au=1:1).

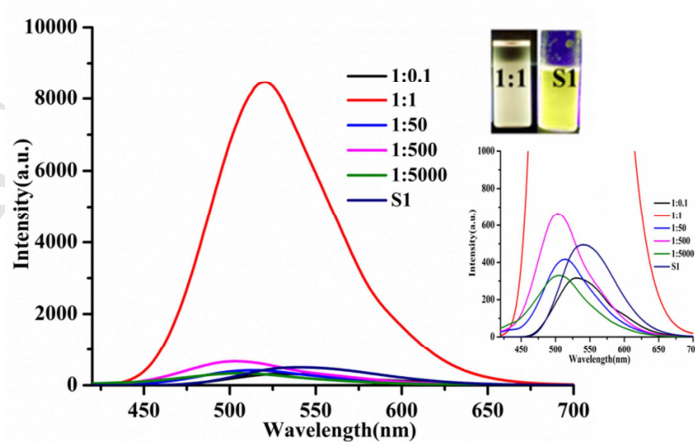


Figure 3 Fluorescence spectra of S1-Au NPs (S1: Au =1:0.1, 1:1, 1:50, 1:500, 1:5000) and S1.

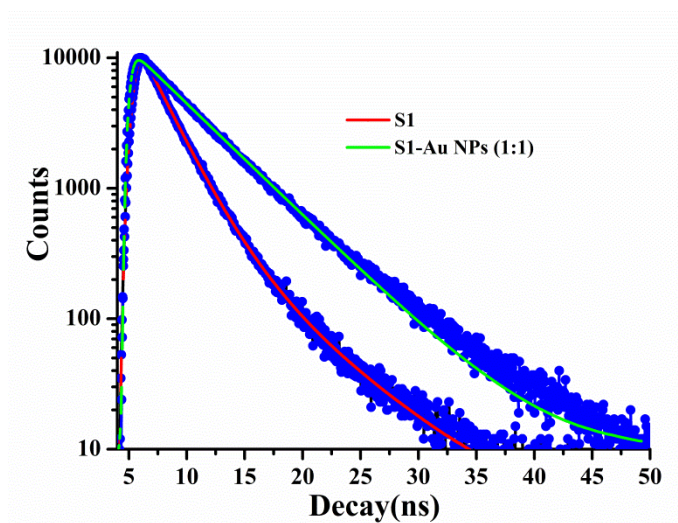


Figure 4 The fluorescence lifetimes of S1 and S1–Au NPs.

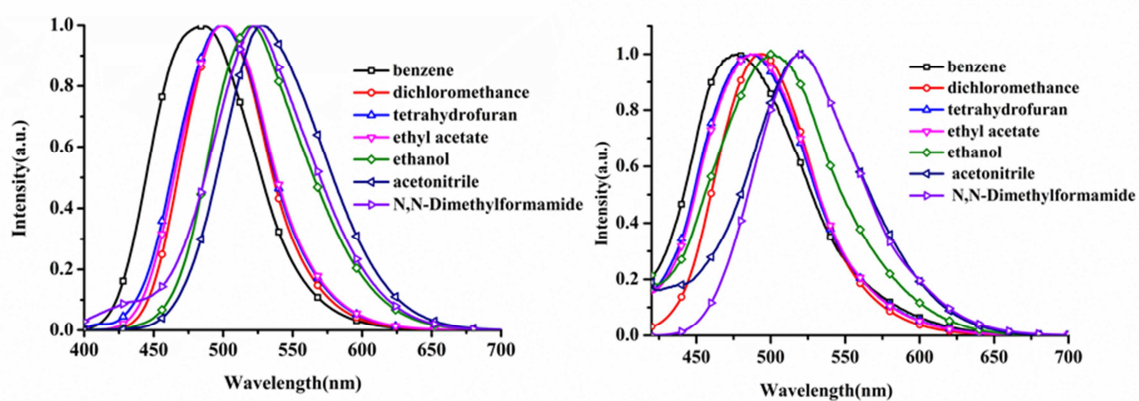
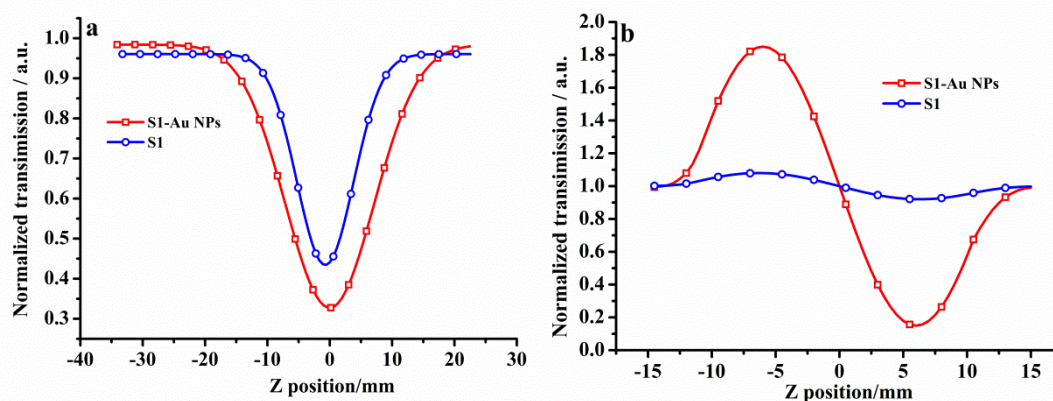


Figure 5 Normalized fluorescence spectra of S1 (left) and S1-Au NPs (right) in different solvents.



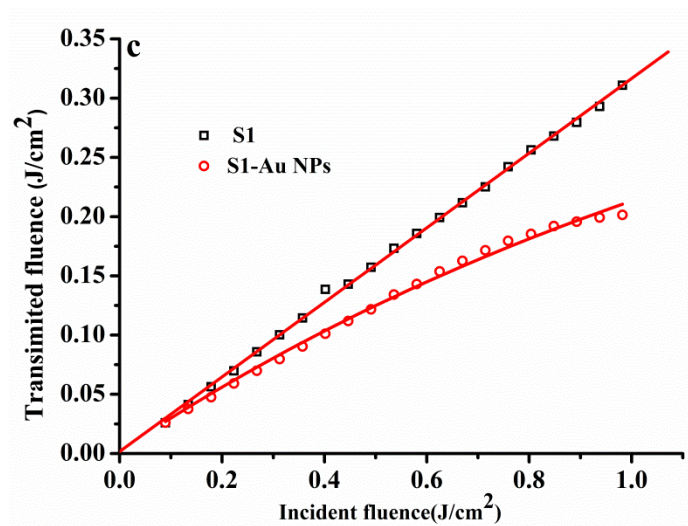


Figure 6 Open (a), closed (b) aperture Z-scan curves, optical limiting (c) of S1 and S1-Au NPs in DMF ($c = 1.0 \times 10^{-3} \text{ mol} \cdot \text{L}^{-1}$)

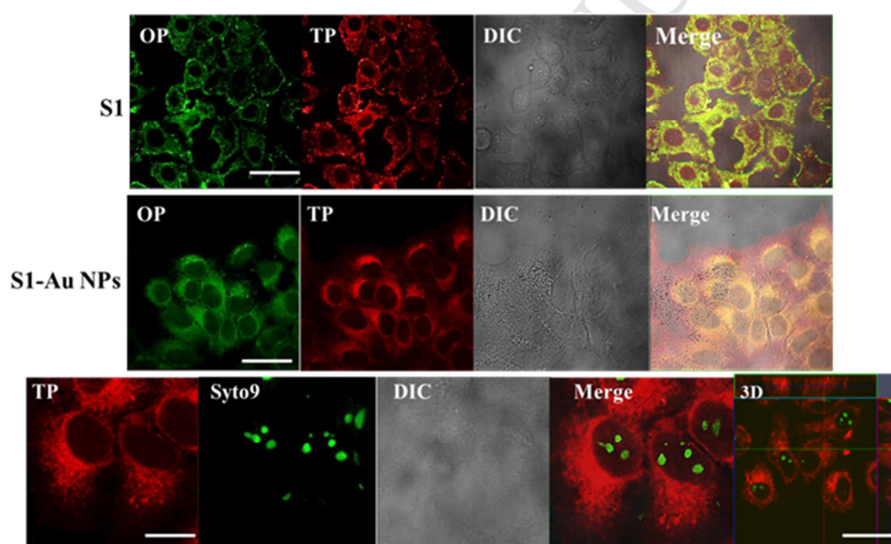


Figure 7 One- and two-photon fluorescence microscopy image of HepG2 cells incubated with S1 and S1-Au NPs, respectively (scale bar: $20 \mu\text{m}$); two-photon fluorescence colocalization imaging (bar: $5 \mu\text{m}$) and 3D image of S1-Au NPs incubated with Syto9 (commercial dyes) ($\lambda_{\text{ex}}=488 \text{ nm}$, $\lambda_{\text{em}}=550 \text{ nm}$).

1. A novel nanostructure material was designed and synthesized by S1 (2, 2': 6', 2''-terpyridyl derivative Zn(SCN)₂ complex) modified gold nanoparticles
2. The coordination reaction mechanism was also studied between Au NPs and the free ligand by the ¹H NMR.
3. Linear absorption and emission spectra had been systematically investigated.
4. The composite material with good nonlinear optical properties had potential applications in vitro cellular imaging.